ASTM INTERNATIONAL

Journal of Testing and Evaluation

Ranjitha Rajagopal,[1] Sameer Sharma,[2] Radhakrishna G. Pillai,[1] and Sankara J. Subramanian[3]

DOI: 10.1520/JTE20160487

Assessment of Stress-Strain Behavior of Corroded Steel Reinforcement Using Digital Image Correlation (DIC)

Journal of Testing and Evaluation

doi:10.1520/JTE20160487 available online at www.astm.org

Ranjitha Rajagopal,[1] Sameer Sharma,[2] Radhakrishna G. Pillai,[1] and Sankara J. Subramanian[3]

Assessment of Stress-Strain Behavior of Corroded Steel Reinforcement Using Digital Image Correlation (DIC)

Reference

Rajagopal, R., Sharma, S., Pillai, R. G., and Subramanian, S. J., "Assessment of Stress-Strain Behavior of Corroded Steel Reinforcement Using Digital Image Correlation (DIC)," *Journal of Testing and Evaluation* https://doi.org/10.1520/JTE20160487. ISSN 0090-3973

ABSTRACT

Understanding the stress-strain behavior of corroded rebars is essential for understanding the structural behavior of corroding reinforced concrete structures. However, conventional methods of testing have several drawbacks, which have led to differences in opinion among researchers regarding the mechanical behavior of corroded rebars. This article proposes an improved method using Digital Image Correlation (DIC) to assess the stress-strain behavior of corroded rebars. The study is conducted in two phases: (a) development of the testing and evaluation method and (b) determination of the mechanical properties (i.e., yield strength, ultimate strength, and ultimate strain) of naturally corroded cold-twisted deformed (CTD) steel rebars using the developed method. The stress-strain behavior of one pristine plain mild (PM) steel and 13 naturally corroded steel rebars collected from a 15-year-old building are investigated in this study. The experimental results show that the proposed method can provide more accurate estimates of mechanical properties than the conventional methods. The developed method facilitates a better understanding of the stress-strain behavior at the fracture location (FL) and other local points of interest on corroded steel rebars. Because DIC measures local strains, the proposed method is able to measure local strain heterogeneity and therefore distinguish between the effects of geometrical variations from those due to true material degradation. This is in contrast to the conventional methods wherein deformation is measured over a finite gauge length, which results in a measurement of average deformation rather than true local deformation. This study emphasizes the need for measurement of full-field deformation to assess the stress-strain behavior of the corroded rebars with highly uneven cross-sectional area.

Keywords

corrosion, Digital Image Correlation, pattern of corrosion, laser scanning, stress-strain behavior

Manuscript received October 4, 2016; accepted for publication May 16, 2017; published online March 13, 2018.

[1] Department of Civil Engineering, Indian Institute of Technology Madras, Sardar Patel Rd., Chennai 600036, Tamil Nadu, India

[2] Department of Engineering Design, Indian Institute of Technology Madras, Sardar Patel Rd., Chennai 600036, Tamil Nadu, India

[3] Department of Engineering Design, Indian Institute of Technology Madras, Sardar Patel Rd., Chennai 600036, Tamil Nadu, India (Corresponding author), e-mail: shankar_sj@iitm.ac.in

Introduction

Corrosion of embedded reinforcement is one of the predominant durability issues faced by reinforced concrete (RC) structures exposed to corrosive environments. Corrosion leads to a reduction in the effective cross-sectional area of the steel rebars, which, in turn, leads to reduction in the load carrying capacity and changes in the structural behavior of the RC structures. To understand and assess the structural capacity and behavior of RC structures experiencing corrosion, it is essential to estimate the influence of corrosion on the stress-strain behavior and the mechanical properties (i.e., yield strength, ultimate strength, and ultimate strain) of the embedded rebars. Several researchers have studied the stress-strain behavior of corroded rebars. However, the literature exhibits considerable differences in opinion regarding the effect of corrosion on the mechanical properties of rebars. Du, Clark, and Chan [1] and Taha and Morsy [2] have reported some of these differences in opinion. **Tables 1** and **2** provide a comparison of the experimental techniques adopted and a comparison of the findings, respectively, from the previous studies. These are also discussed in the following sections.

EFFECT OF CORROSION ON YIELD STRENGTH

In literature, the term strength is defined either in terms of force (in kN) or stress (in MPa). Throughout this paper, strength refers to the capacity of the rebars in units of stress (MPa). Researchers have evaluated the strength properties of corroded rebars in two different ways: (a) the strength computed for the corroded rebars using the nominal diameter of the specimen, referred to as the "nominal strength," and the strength computed using the residual cross-sectional area (after corrosion) of the specimens, referred to as the "actual strength" in this article. The nominal strength of corroded rebars gives an idea of the variation in the strength of the rebars from the expected design value of pristine rebars, whereas the actual strength gives the strength of the residual intact steel.

Researchers have reported that nominal yield strength of rebars decreases significantly with increase in degree of corrosion [1,3–5]. This is due to the use of nominal cross-sectional area in the denominator while computing stress rather than the residual cross-sectional area. Du, Clark, and Chan [1] and Apostolopoulos and Papadakis [4] reported that the reduction in nominal strength is not proportional to the reduction in cross-sectional area, suggesting that the corrosion may induce more effects in the bulk material than just a reduction in cross-sectional area. However, researchers differ in their opinion regarding the actual yield strength of corroded rebars. A few of the researchers have stated that corrosion has no significant effect on the actual yield strength of the rebars [4,6]. However, Du, Clark, and Chan [1] reported that actual yield strength reduces by 5 % with 10 %

TABLE 1 A review of the experimental techniques adopted in the previous studies.

Method of Inducing Corrosion	a) Method of Measuring Residual CSA b) Length Over Which Average CSA Is Measured	a) Stressed/Unstressed Specimens b) Pattern of Corrosion	Diameter of the Specimen	Selected Gauge Length	Reference
Impressed current technique	a) Mass loss method b) Mass loss method c) NR	Unstressed NR	6 and 12 mm	NR	Almusallam [3]
Naturally corroded specimen	a) Vernier calipers and average CSA loss b) 25 mm	Stressed Pitting	16 mm	25 mm within 75 mm	Palsson and Mirza [7]
Impressed current technique	a) Liquid displacement technique b) 10 mm	Unstressed NR	8, 16, and 32 mm	50 mm	Du, Clark, and Chan [1]
Machined notches and anodic polarization	a) Weight loss method for lightly corroded and liquid displacement for heavily corroded specimens b) NR	Unstressed Uniform and localized	12, 16, 20, and 24 mm	Five times the diameter	Cairns et al. [6]
Salt spray technique	a) Mass loss b) 250 mm	Unstressed NR	10 mm	150 mm	Apostolopoulos and Papadakis [4]
Long-term exposure to chlorides mixed with concrete	a) Mass loss after tension testing b) Depending on the corrosion pattern, shortest being 5 mm	Stressed Pitting	16 mm	200 mm	François, Khan, and Dang [5]

Note: CSA, cross-sectional area; NR, not reported; NA, not applicable.

TABLE 2 A summary of the effect of corrosion on the mechanical properties of rebars from the literature.

Yield Strength		Ultimate Strength				
Nominal	Actual	Nominal	Actual	Ultimate Strain	Elastic Modulus	Reference
NR	Marginal decrease	NR	Marginal decrease	Decreases	NR	Almusallam [3]
NR	No change	NR	No change	Decreases	NR	Palsson and Mirza [7]
NR	Reduces	NR	Reduces	Decreases	NR	Du, Clark, and Chan [1]
NR	No change	NR	Decreases	Decreases	NR	Cairns et al. [6]
Decreases	No change	Decreases	Reduces	Decreases	NR	Apostolopoulos and Papadakis [4]
Reduces	No change	Reduces	Increases	Decreases	No change	François, Khan, and Dang [5]

Note: NR, not reported.

reduction in cross-sectional area (measured using weight loss method). On the other hand, Palsson and Mirza [7] evaluated a set of naturally corroded rebars collected from a demolished overpass and reported "a slight increase in the yield stress was noted in the case of the pitted specimens." This could be due to the measurement of average loss in cross-sectional area that does not provide an estimate of the actual cross-sectional area at the fracture location (FL) or the pit.

EFFECT OF CORROSION ON ULTIMATE STRENGTH

Similar differences in opinion are observed in the reported effects of corrosion on the ultimate strength of unstressed rebar specimens. Almusallam [3], Apostolopoulos and Papadakis [4], and François, Khan, and Dang [5] concluded that the nominal ultimate strength is reduced, while actual ultimate strength remains unaffected by corrosion. This is also due to the use of nominal cross-sectional area instead of the actual residual cross-sectional area. On the other hand, Du, Clark, and Chan [1] reported a marginal reduction of 6 % in actual ultimate strength because of 10 % corrosion. Apostolopoulos and Papadakis [4] reported, "the actual effect of corrosion on the tensile strength properties of the reinforcing steel is moderate." Cairns et al. [6] reported an apparent increase in the measured ultimate strength with increasing degree of corrosion. Cairns et al. [6] explained this unexpected observation as the following:

> If a bar does not have a completely uniform cross section and material composition throughout its length, then it would clearly be expected to fracture at the point where the material is weakest. If the position of the pit does not coincide with the location where the steel is weakest, an apparent increase in strength (where this is based on the minimum cross-sectional area) will be measured.

Later, François, Khan, and Dang [5] reported an increase in ultimate strength in corroded rebars, which was explained as "almost all the corroded bars failed at a pit location and the increase in true ultimate strength at the pit can be explained by the fact that the failure path is imposed by the pit and does not correspond to the weakest point of the steel bar as is the case for non-corroded bar." However, it seems that an in-depth statistical analysis with a larger set of similar specimens might have led to a different conclusion.

These comments show that there are considerable differences in opinion among researchers regarding the effect of corrosion on the strength properties of rebars. Du, Clark, and Chan [8] have reported that the differences in opinion in the previous studies are mainly due to differences in the experimental techniques adopted. The possible reason for these differences in opinion could be the following.

- The fracture of the specimen may occur at a location away from the pit or the location with least cross-sectional area because of some internal defect in the material. However, the strength could be computed with the measured least cross-sectional area, leading to a measured increase in strength properties.
- The residual cross-sectional area estimated using the mass loss or liquid displacement method gives only an average reduction in the cross-sectional area over a certain length of the specimen. This value may be significantly different from actual residual cross-sectional area at FL, especially if the cross-sectional area profile is highly uneven. This may lead to underestimation of the actual reduction in the cross-sectional area at the FL, which might lead to measurement of a decrease in the strength properties.

EFFECT OF CORROSION ON ULTIMATE STRAIN

Although differences in opinion regarding the strength properties exist, researchers agree that the ductility (expressed in terms of ultimate strain) reduces because of corrosion. Note that the ultimate strain is measured using an extensometer over a gauge length selected by the user. Apostolopoulos and Papadakis [4] and Cairns et al. [6] concluded that the ductility decreases exponentially with increasing degree of corrosion. Almusallam [3] reported that the reduction in the measured ductility is due to stress concentration at the locally thinned or corroded section, thus leading to a lower effective strain (measured over the entire gauge length) at the time of fracture. Palsson and Mirza [7] reported that the reduction in measured ductility occurs because only a shorter segment of the gauge length would yield compared to that

of the pristine rebars. The reduction of ductility in specimens with pitting corrosion was reported to be more than that in specimens with uniform corrosion [9,10]. Zhu and François [10] reported that this behavior is due to the eccentricity of the center of gravity of the cross-section to the axis of the applied force, which could induce local bending and reduce the ultimate strain.

One of the problems associated with the measurement of the ductility of the corroded rebars is the "arbitrary" selection of gauge length. The strain is measured using extensometers as $\varepsilon = \Delta l/L_0$, where Δl is the change in length and L_0 is the gauge length over which strain is measured. ASTM E8M, *Standard Test Methods for Tension Testing of Metallic Materials* [11], recommends a gauge length of five times the nominal diameter (i.e., 5Φ) for the rounded test specimens. In the case of corroded rebars, the difficulty in visually predicting the FL compels researchers to use a suitable gauge length based on the number and distribution of probable FLs (and to measure an average reduction in residual cross-sectional area). Different suitable gauge lengths selected in the previous studies are presented in the fifth column of **Table 1**. For example, Palsson and Mirza [7] have measured strains on 16-mm diameter rebar over two different nested extensometers—one with 25-mm gauge length within 75-mm gauge length. On the other hand, Du, Clark, and Chan [1] adopted 50-mm gauge length for 8-, 16-, and 32-mm diameter rebars; Apostolopoulos and Papadakis [4] used 150-mm gauge length for 10-mm diameter rebars; and François, Khan, and Dang [5] used 200-mm gauge length for 16-mm diameter rebar.

The arbitrariness of the gauge section length is itself not problematic if the underlying deformation was homogeneous. However, because rebars have a complicated geometry, and often local material degradation, the resulting strain deformation (especially at failure) is highly localized. Under such circumstances, the gauge length plays a critical role in the computed strains. With longer gauge lengths, more of the areas with low strains are included in the averaging, resulting in a lower overall strain value, and vice versa. One can obtain different strain results for the same heterogeneous deformation fields simply by changing gauge lengths. Thus, the use of extensometers for heterogeneous strain fields is a fundamentally flawed approach.

CURRENT RESEARCH NEED

The use of average residual cross-sectional area along the length of the specimen and the selection of large gauge lengths are the major drawbacks associated with the conventional methods of evaluating corroded rebars. The former causes stress to be estimated incorrectly from the applied loads, whereas the latter leads to incorrect measurement of strains. If either the stress or the strain is wrong, then the material behavior inferred from such conventional studies will also likely be incorrect, e.g., one may conclude that the material has undergone degradation while in fact, the stress or strain, or both, are incorrectly estimated due to purely geometrical changes. Therefore, there is a need to address both of these issues in order to arrive at the right conclusion regarding material degradation. Several researchers have already tackled the cross-sectional area measurement issue. Kashani, Crewe, and Alexander [12] have used a structured light scanner to compute the cross-sectional area along the rebars and hence the surface pitting pattern on them. Apostolopoulos, Demis, and Papadakis [13] employed image analysis methodology for a reliable pit depth and area measurement on corroded specimens. The average pit depth and area of the pit were calculated from stereoscopic images taken at the pit location using 35× magnification lens based on the grayscale intensity. It is evident that to draw the correct conclusions regarding rebar material degradation, any research study should include the following components:

- a more accurate estimation of the residual cross-sectional area along the rebars, which in turn will facilitate accurate prediction of the probable FL(s) on corroded rebars with uneven cross-sectional area,
- a posteriori analysis to compute the local deformation at or near the fractured location, and
- the ability to capture the strain heterogeneity because of unevenness of the cross-sectional area of the corroded rebars.

Considering these requirements, this study proposes an improved method of evaluating mechanical properties of corroded rebars using Digital Image Correlation (DIC), which is a non-contact, optical technique for measurement of full-field deformations over the surface of a deforming specimen [14]. The measurement of full-field deformation can overcome the limitations of the conventional methods of measuring the effective strain over a gauge length using extensometers. Because deformations are available over a user-defined spatial domain, one can capture the strain heterogeneity along the length of the rebars. Full-field deformation measurement also aids in estimating the strain at the FL more accurately, which gives a better estimate of the stress-strain behavior of corroded rebars. The proposed method also incorporates 3D laser scanning to estimate the residual cross-sectional area profile along the corroded rebars at very closely spaced intervals, which can facilitate an accurate identification of the FL (prior to the tension test). DIC has been recently gaining wide acceptance in the field of civil engineering to monitor live structures as well as in laboratory studies. For example, DIC has been employed to measure displacements in a longitudinal truss girder of a steel railway bridge in Poland [15], to study brittle failure of prestressed concrete structures [16], to measure the shear capacity of the I-shaped prestressed concrete beams [17], and to measure crack opening in a loaded RC bar [18].

In the next section, the research significance of this study is discussed. Then an overview of the experimental program is provided. Then the steps involved in the specimen preparation, tension testing, and data analysis of the rebars using the proposed

method are explained in detail. Following this is the section on the evaluation of the stress-strain behavior and mechanical properties of a set of corroded rebars using the developed method. After this, the conclusions drawn from this study, the applications, and the limitations of the developed method are presented.

Overview of the Experimental Program

This study consists of two phases. The first phase involves the development of the testing and evaluation method using two-dimensional DIC (2D-DIC) technique, and the second phase involves the determination of the mechanical properties of a set of corroded rebars using the developed method. Broadly, two types of steel rebars are used in this study: plain mild (PM) steel rebars and cold-twisted deformed (CTD) steel rebars, as shown in **Fig. 1**. The typical chemical composition of PM and CTD steel is presented in **Table 3**. One pristine PM steel rebar and 13 corroded CTD rebars were collected from a 15-year-old building. **Fig. 2** shows the testing region and the residual cross-sectional area at the FL of the 14 specimens tested for this study. The details of the specimens used for the two phases of this study are presented in **Table 4**.

The first phase of this study deals with the formulation of the steps involved in the testing of corroded rebars and assessment of their stress-strain behavior. Some of the experimental procedures involved are conventionally practiced, while others were decided based on multiple trials. The PM steel rebar specimen has a uniform cross-sectional area, without any ribs, and negligible corrosion. Three naturally corroded CTD rebar specimens have varying degrees of corrosion: 3, 18, and 33 % (computed as explained later in the section "Quantitative Estimation of Degree of Corrosion"), as shown in **Fig. 2**.

The second part of the study involves the evaluation of the stress-strain behavior and mechanical properties of ten additional naturally corroded CTD rebars specimens (as shown in **Fig. 2**) with the degree of corrosion varying from 3–40 % (computed as explained later in the section "Quantitative Estimation of Degree of Corrosion"). CTD rebars were chosen for this study because several structures built using CTD rebars could be experiencing severe corrosion now. The assessment of the stress-strain behavior of corroded CTD rebars would help to assess the structural performance of the existing corroding structures.

Phase I: Development of Test and Evaluation Method

The following subsections illustrate the procedure for specimen preparation, the input parameters selection for the measurement of full-field displacement using DIC technique, and the computation of strain from the full-field deformation to plot the stress-strain curve of rebars.

PREPARATION OF TEST SPECIMENS

The rebars were cut into 420-mm-long (16.53 in.) specimens. The corrosion products were removed from the surface of the specimen as per the procedures recommended in ASTM G1-03, *Standard Practice for Preparing, Cleaning, and Evaluating Corrosion Test Specimens*. The cleaning solution was prepared by mixing 500 mL (0.0017 ft^3) of hydrochloric acid with 3.5 g

FIG. 1
Typical plain mild (PM) steel (a) and cold-twisted deformed (CTD) steel rebars (b). Image was taken by the authors.

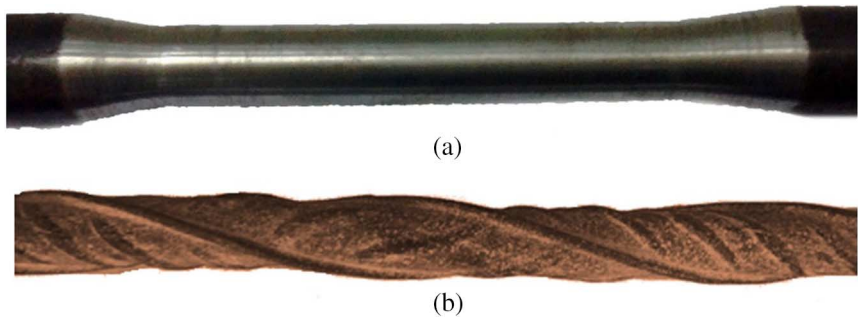

TABLE 3 Chemical composition of plain mild (PM) steel and cold-twisted deformed (CTD) steel.

Elements	Cu	Co	Al	Ni	Mo	Cr	S	P	Mn	Si	C	Fe
PM	0.27	–	–	0.09	0.02	0.08	0.05	0.06	0.64	0.26	0.19	Re
CTD	0.09	0.01	0.01	0.07	0.01	0.07	0.27	0.09	0.45	0.23	0.13	Re

Note: Re, remaining.

FIG. 2 PM steel and corroded CTD rebar specimens with the degree of corrosion varying from 3–40 %. Note: The dotted lines indicate the FL on these specimens. The cross-sectional area at the FL (before the tension test) is shown above corresponding specimens. The specimen ID and the degree of corrosion (provided inside parentheses) are marked on the top of each specimen. "P I" and "P II" represent Phase I and Phase II of this study.

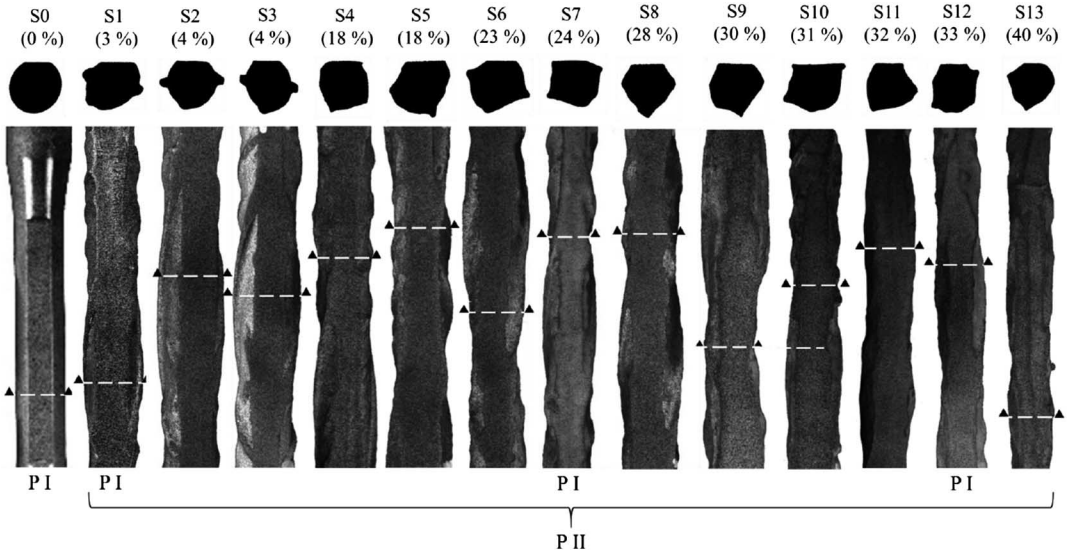

TABLE 4 Details of the specimens used in this study.

Steel Type	Specimen ID	Degree of Corrosion (%)	Phase I (PI)	Phase II (PII)
Plain mild (PM) steel	S0	0	✓	
Cold-Twisted Deformed	S1	3	✓	✓
(CTD) steel	S2	4		✓
	S3	4		✓
	S4	18		✓
	S5	18		✓
	S6	23		✓
	S7	24	✓	✓
	S8	28		✓
	S9	30		✓
	S10	31		✓
	S11	32		✓
	S12	33		✓
	S13	40	✓	✓

(0.0077 lbs) of hexamethylenetetramine and diluted with distilled water to 1,000 mL (0.035 ft^3). Specimens were immersed in this solution for ten minutes and the rebars were cleaned using a wire brush. This process was repeated until the corrosion products were completely removed. 2D-DIC, which is employed in this study, involves only one camera and is suitable only for measuring deformations on flat specimens. Therefore, as shown in **Fig. 3a**, the specimens were milled for approximately 0.5-mm (0.019 in.) depth, to obtain a plane surface of approximately 5–7-mm (0.196–0.275 in.) width. A typical tension test specimen of 12-mm (0.472 mm) diameter was made from 16-mm (0.629 in.) diameter PM steel rebar with a parallel length of 60 mm (2.36 in.) to the center of the 420-mm-long (1.378 ft) specimens (as shown in **Fig. 1**). The next step was to estimate the residual cross-sectional area profile of the corroded specimens to identify the probable FL.

ESTIMATION OF RESIDUAL CROSS-SECTIONAL AREA

To obtain a more accurate estimate of the residual cross-sectional area at closer intervals along the length of the corroded specimen, different techniques were attempted, such as wax imprinting, liquid displacement technique, and 3D laser scanning technique. The 3D laser scanning technique provided the most accurate estimate of residual cross-sectional area at very close intervals along the rebar. A 3D model of the milled specimen was created using the laser scanning technique (see **Fig. 3b**). In this study, an LPX-600 3D laser scanner (Roland DG Corporation, Japan) with an accuracy of ±0.05 mm (±0.002 in.) was used to scan the specimens. The scanner can detect only white or light colored objects. Hence, the milled specimens were painted in white before scanning. A suitable longitudinal and circumferential pitch of 1 mm (0.039 in.) and 0.32 mm (0.0126 in.), respectively, was selected depending on the accuracy needed for the measured cross-sectional area. **Fig. 3b** shows a 3D model of the specimen created using the laser scanning technique. From the digitized 3D model of the specimen, the cross-sectional area at every 1 mm (longitudinal pitch of scanning) along the length of the specimen is computed using a MATLAB® (MathWorks, Natick, MA) code. The location with the least cross-sectional area was identified

FIG. 3

Specimen preparation process: (a) milled surface on the specimen, (b) 3D model of the specimen obtained using laser scanning technique, (c) speckling using black and white spray paints, and (d) speckles on the milled surface of the specimen. Image was taken by the authors.

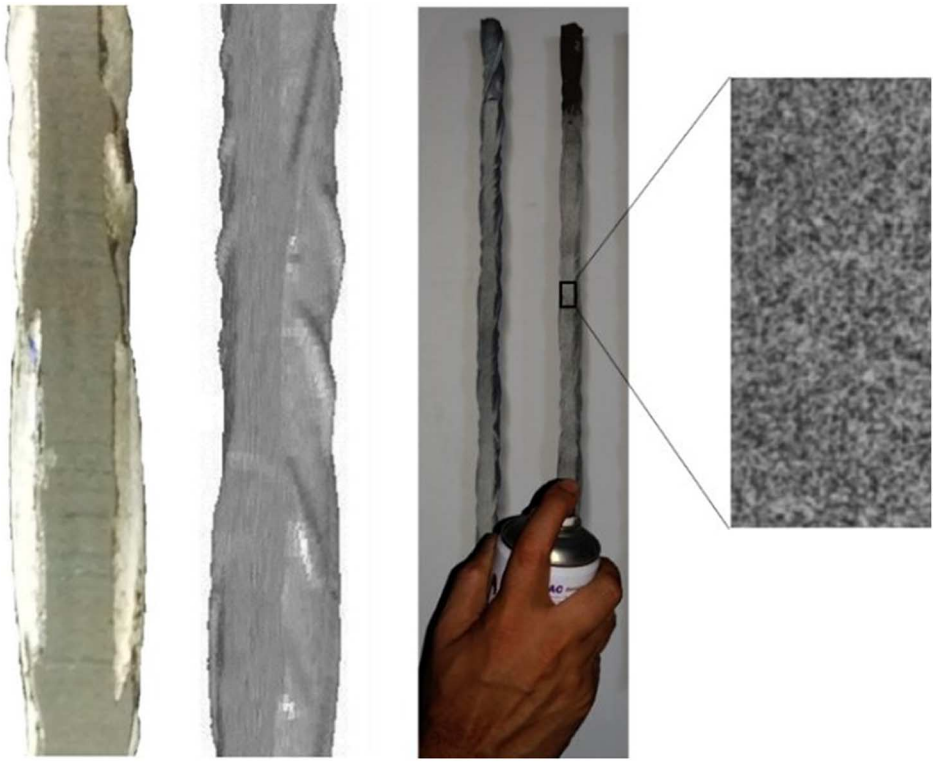

as the most probable FL. In this study, FL refers to the 1-mm-thick slice of the specimen in which the specimen fractured under tension. The FL of all the specimens (except S1 and S2, with the least degree of corrosion) after the tension test coincided exactly with the identified probable FL.

SELECTION OF AREA OF INTEREST

Area of Interest (AOI) is the predefined region on the surface of the specimen where deformations are to be measured. The AOI for test specimens is selected prior to testing, such that the predicted FL is approximately at the center of the selected region. This is done so that strain distribution to either side of the FL can be captured. ASTM E8M-13a, *Standard Test Methods for Tension Testing of Metallic Materials*, recommends a gauge length of 60 mm (2.36 in., which is equal to five times the diameter) for the specimens with 12-mm (0.472 in.) diameter. Therefore, in this study, a region of 60-mm (2.36 in.) length is selected as the AOI such that the identified probable FL lies approximately at the middle of the selected region.

SPECKLING OF SPECIMENS

The measurement of displacement using DIC involves image subsets correlation across a set of images acquired during the specimen deformation. This process is discussed in detail later in "Computation of Full-Field Displacement Using DIC." For this process, the DIC program should be able to distinguish each image subset in the AOI without the ambiguity across all images. To facilitate subset-to-subset correlation, the milled surface of the specimen was speckled with a random distribution of dark and light blobs (defined as speckles) using spray paints of contrasting colors (white and black). It was ensured that the blobs were discontinuous, rather than a continuous layer on the steel rebar surface.

TENSION TESTING AND IMAGE CAPTURING

Fig. 4a shows the experimental setup for tension testing of the corroded rebar specimens and for capturing the images for posterior DIC strain computations. The experimental test setup includes a tensile testing machine of 1,000 kN (224.81 kip) capacity with a live upper jaw/end and a dead lower jaw/end, a QICAM 1394 Firewire camera (QImaging, Surrey, Canada) (1,392 by 1,040 pixel resolution, 4.65 μm-pixel size) with a Nikkor 50 mm f/1.8D lens (Nikon, Tokyo, Japan) to capture images of the specimen during the tension test at uniform time intervals (one image per second, in this study), and electric lamps to provide illumination of the specimen. The camera is placed in front of the specimen such that focal plane of the camera is parallel to the AOI (or the milled surface). **Fig. 4b** shows two images of the specimen taken: one at the beginning of the test and the other just before fracture of the specimen. Points A and B mark the top and bottom

FIG. 4 Capturing of images during deformation of test specimens: (a) experimental setup and (b) setting of camera frame.

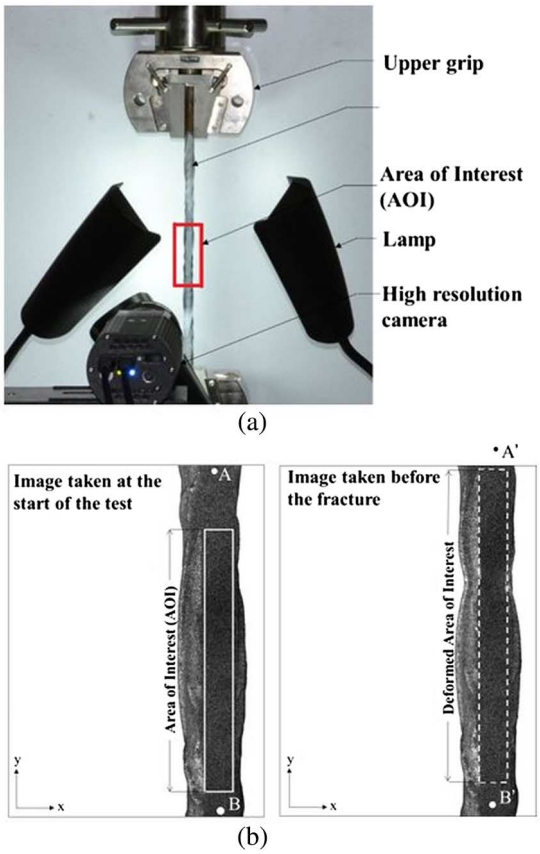

of the viewing area of the camera. As the specimen deforms under tension, the top part of the specimen moves out of the frame (Point A' is out of the viewing area in the second image in **Fig. 4b**). Hence, the camera frame is positioned leaving adequate margin towards the live jaw/end in the AOI, to ensure that the AOI remains in the viewing area of the camera till the specimen fractures. The distance between the points A and B is recorded before the test to calibrate the images. The tensile test is conducted at a displacement rate of 2 mm/minute (0.0013 in./s), which complies with the strain rate recommendation as per IS 1608, *Mechanical Testing of Materials – Tensile Testing* (Bureau of Indian Standards 2005). The images of the AOI are captured at the rate of one image per second till the specimen fractures. The number of images captured per specimen during the tensile test (till fracture) ranges from approximately 600 for the severely corroded specimens to 1,200 for the least corroded specimens.

QUANTITATIVE ESTIMATION OF DEGREE OF CORROSION

In this study, the degree of corrosion of each specimen is computed based on the reduction (in percentage) of the cross-sectional area because of corrosion at the fractured location (identified after the tension test) compared to the nominal

FIG. 5 Initial and residual cross-sectional areas of the corroded rebar specimens.

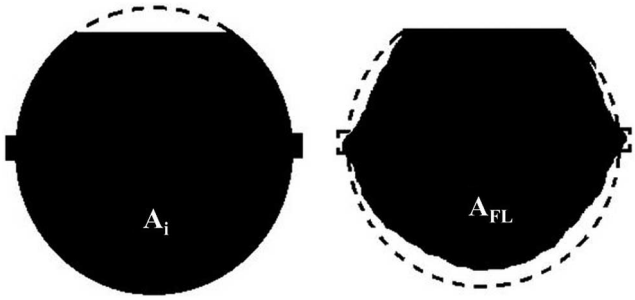

cross-sectional area of the as-received specimen after milling. **Fig. 5a** and **5b** shows the original cross-sectional areas of the as-received specimen (A_i) and the residual cross-sectional area at the FL of the corroded specimen (A_{FL}). The degree of corrosion is computed as given in Eq 1:

$$\text{Degree of corrosion } (\%) = \frac{A_i - A_{FL}}{A_i} \times 100 \quad (1)$$

A_i is computed by deducting the area of the segment removed by milling from the nominal cross-sectional area, as shown in **Fig. 5a**. A_{FL} is computed from the virtual 3D laser scan model of the specimen. **Table 5** presents the degree of corrosion of all 13 corroded CTD rebar specimens (used in the first and second phase of this study).

COMPUTATION OF FULL-FIELD DISPLACEMENT USING DIC

The full-field displacement in the specimen was calculated using DIC from multiple images of the AOI captured during the tension test. This process is illustrated in **Fig. 6** (adapted from Pan et al. [19]). The figure shows the configuration of a deforming region in the undeformed and deformed state. The movement of the point of interest is estimated by locating the point in the reference configuration (i.e., the image of the specimen taken at the start of the test which corresponds to the undeformed state) and tracking its corresponding location in the next image containing the deformed state of the specimen. This is illustrated in **Fig. 6** as points P and Q occupying the spatial coordinates (x_0, y_0) and (x_1, y_1) in the undeformed state (reference configuration) and the spatial coordinates (x_0', y_0') and (x_1', y_1') in the deformed configuration of the specimen. Once the point correspondence is known between the two frames (the reference and the current state), the full-field displacements are computed by comparing the position of every point in the deformed image with the corresponding position in the reference image [12].

After the tension test, the images were analyzed using the commercial DIC software Vic-2D^{TM} (Correlated Solutions Inc., Irmo, SC) to determine the full-field displacements u and v along the X (transverse) and Y (longitudinal) directions. Optimized

TABLE 5 Computation of degree of corrosion in the test specimens.

Specimen ID	A_0 (mm^2)	Area of the Segment Milled Off (mm^2)	A_i (mm^2)	A_{FL} (mm^2)	Degree of Corrosion (%)	Rate of Change of Cross-Sectional Area at Fracture Location (dA/dy)
1		5.1	111.1	107.2	3	0.96
2		4.4	111.8	107.6	4	0.96
3		2.7	113.5	109.2	4	0.97
4		2.6	113.6	92.7	18	0.90
5		3.1	113.1	92.3	18	0.94
6		3.6	112.7	87.1	23	0.86
7	116.2	3.1	113.1	85.4	25	0.92
8		2.4	113.8	81.6	28	0.90
9		4.9	111.2	77.4	30	0.73
10		3.5	112.7	77.9	31	0.81
11		3.9	112.3	75.9	32	0.83
12		4.5	111.7	75.1	33	0.78
13		3.7	112.5	67.3	40	0.81

FIG. 6 Schematic diagram illustrating the principles of DIC (adapted from Pan et al. [19]).

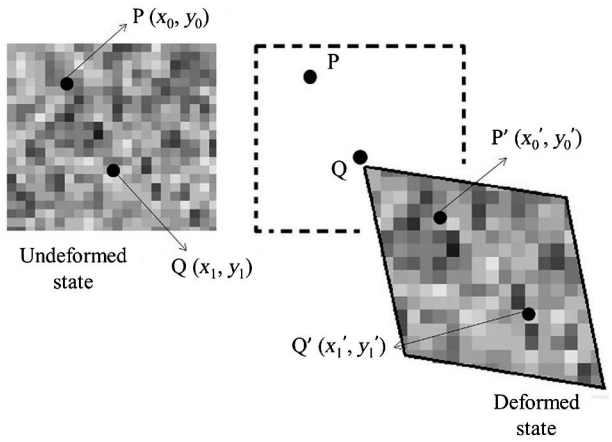

8-tap filter interpolation and zero-mean normalized sum of squared difference correlation criterion with Gaussian subset weights were used in all our analyses. Before the images are correlated to compute displacements, two DIC parameters have to be selected: the subset size (SS) and the step size (ST). The SS refers to the size of the sub-image used in the DIC computations, each of which gives the displacement vector at the center of the subset. The ST refers to the distance between neighboring displacement measurement locations. For example, a 25 by 25 subset with a ST of 10 pixels means that 625 intensity values participate in the computation of the displacement vector at the center of the subset, and one obtains one such computed displacement vector every 10 pixels along the X and Y directions. The SS is generally determined by the average speckle size in the image. In our work, we estimate the average speckle size using an autocorrelation method and choose the SS to be 15 pixels, which is approximately three times the speckle size, as recommended by a widely followed rule of thumb. We also chose the ST to be 15 pixels so that neighboring subsets did not share any pixels, thereby leading to uncorrelated displacement errors [20]. For our studies, 15 pixels corresponds to about 0.8 mm, so we obtain one displacement measurement at this spacing. Autocorrelation function [21] was used to a compute speckle size of 4 pixels, thus a SS of 15 pixels (≈ three times the speckle size) was used throughout our study, as shown in **Fig. 7**.

COMPUTATION OF STRAIN

In general, the displacements resulting from full-field experimental techniques, such as DIC, are corrupted with noise, and therefore the displacements are smoothed prior to numerical differentiation. The parameter that controls the amount of smoothing in Vic-2D™ is the filter size, which determines the number of neighboring displacement data points used to compute strains. If filter size is large, displacements get over-smoothed and strain heterogeneity is lost. On the other hand, if it is too small, the noise in the displacement data leads to erroneous strain computation. **Fig. 8** presents a typical image of the AOI taken in this study. Out of 1,037 by 1,391 pixels in the image, an approximately 80-mm length of the specimen occupies 220 by 1,391 pixels. The selected AOI occupied approximately 120 by 1,100 pixels. Using a ST of 15 pixels, the size of the displacement field data is 8 by 73. Hence, even the smallest filter size of 5 available in Vic-2D™ would result in considerable amount of oversmoothing.

Recently, Grama and Subramanian [22] proposed a new strain computation method using Principal Component Analysis (PCA). In this method, the prime variations in the displacements are captured using a few (<< rank of the displacement matrices) one-dimensional singular vectors, often called the dominant singular vectors, which are systematically smoothed and differentiated for computing the strains. In the process of reconstructing the displacement using a few singular vectors, dimensional reduction (the conventional 2D plane or 3D surface is converted to a simpler 1D curve fitting of series of the dominant singular vectors) and data denoising are also achieved.

In the present work, strains are computed using the PCA based technique. The number of dominant singular vectors is identified by inspecting the logarithmic singular values, which are smoothed using Legendre polynomials for computing displacement gradients [22]. Reu [23] suggests a virtual strain gage (VSG) study to choose optimum DIC parameters such as SS, ST, and strain window (SW). The study is performed by first selecting three images: a reference image, an unloaded noise image, and a maximum deformation image. Computing strains for the unloaded noise image with respect to the reference image (which is also unloaded) yields the measurement resolution. In our work, we use a PCA-based strain computation approach, in which the conventional SW is replaced by a filter size used in the differentiation

FIG. 7 Selection of DIC parameters using Virtual Strain Gage study. (a) Strains are extracted along a line containing the failure location (i.e., maximum strain region). (b) A range of DIC parameters is chosen for the VSG study, and strains are computed at each of the parameter combinations. The increase in the strain window (or filter size) results in smoothing of the maximum strain, and PCA strains have excellent agreement with the lowest strain window.

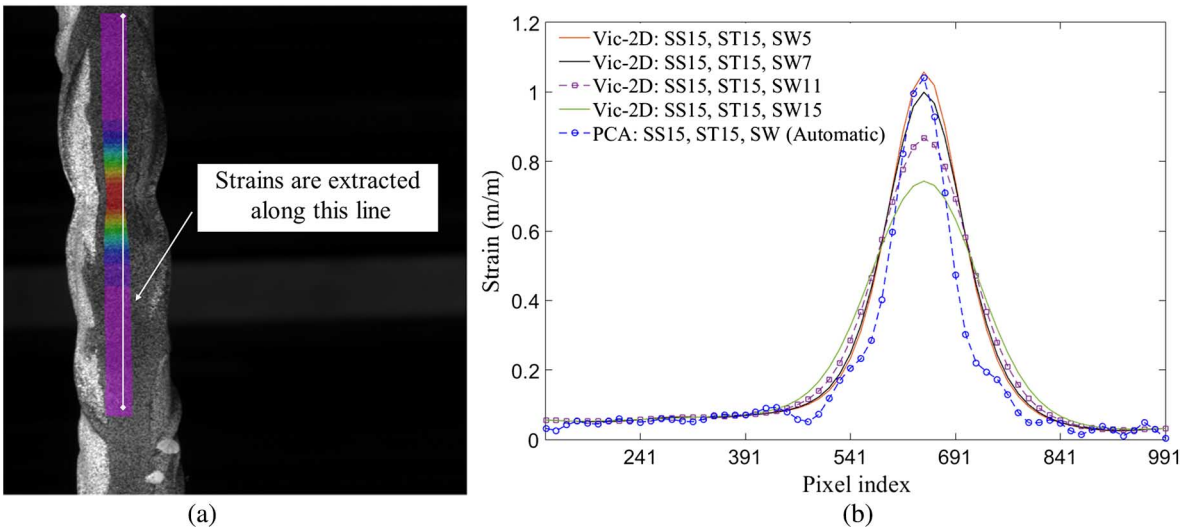

FIG. 8 Pixels occupied by the specimen and the AOI in the image.

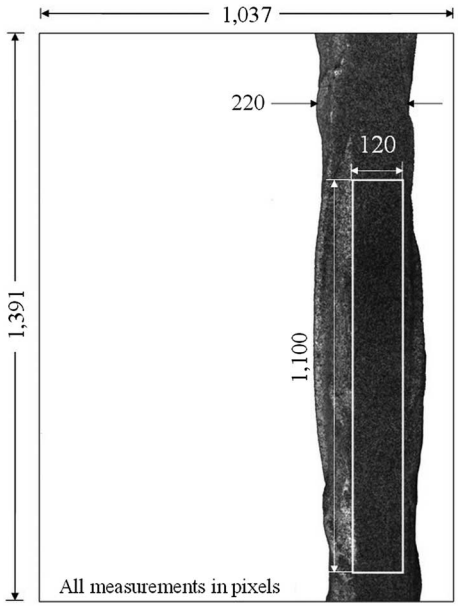

of 1D singular vectors. However, unlike the conventional strain computation workflow used by commercial packages such as Vic-2D, this filter size is not a variable; instead, it is chosen automatically using the Bayesian Information Criterion [24]. Therefore, we perform a modified VSG study as follows:

(a) Measure displacements using Vic-2D with SS = 15 and ST = 15.
(b) Compute strains using Vic-2D for SW = 5, 7, 11, and 15.
(c) Compute strains using our PCA-based method.
(d) Compare strain results from (b) and (c).

Table 6 summarizes our VSG study, from which we conclude the following:

(a) The measurement resolution of the Vic-2D strain is 12–20 μ, while it is 1.4 μ for the PCA strain computation.
(b) The Vic-2D results show that one can have good spatial resolution or good measurement resolution, but not both for any DIC parameter combination.
(c) On the other hand, the PCA-based strain computation results in superior spatial and measurement resolutions and hence can be considered as a better choice for computing strains for the performed experiments.

An important point of discussion is the applicability of 2D-DIC to the present study. It is well understood that 2D-DIC is strictly applicable only to planar specimens undergoing in-plane deformations. If these conditions are violated, errors are introduced into the measured in-plane deformations. Sutton, Orteu, and Schreier [14] and Sutton et al. [25] report that the error that occurs because of out-of-plane displacements in the in-plane strain measurements can be estimated by the ratio ($\Delta z/z$), where Δz is the out-of-plane displacement and z is the object standoff distance from the lens pinhole. We estimate z using the focal length of the lens f, the physical size of the sensor h, and object size l as Eq 2:

$$z = l \times \frac{f}{h} \tag{2}$$

In our experiments, f = 50 mm, h = 4.836 mm (1,392 pixels by 4.63 μm), and $l \approx 80$ mm, leading to z = 827 mm. Next, we

TABLE 6 Virtual gauge study (VSG) for the uniaxial tension test.

Parameters	Vic-2D				PCA
Strain window (SW)	5	7	11	15	Polynomial order = 4
VSG = $[(SW-1)\times ST]+1$	61	91	151	211	46
Spatial resolution (SR) = $[(SW-1)\times ST]+SS$	75	105	165	225	60
Measurement resolution (μ)	20.1	18.2	15.6	12.6	1.39

estimate the out-of-plane motion Δz from the Poisson contraction of the specimen as given in Eq 3:

$$\Delta z = -\nu \times \varepsilon f \times r \tag{3}$$

where:

ν = the Poisson's ratio,

f = the strain at failure, and

r = representative radius of the bar. With $\nu = 0.5$, $\varepsilon f = 1.1$, and $r = 6$ mm, $\Delta z \approx 3$ mm, leading to an in-plane strain error of 3/827 = 3,600 μ. In addition to the Poisson contraction, additional out-of-plane motion could also result in specimen rotation and translation during the experiment. However, because we used a stiff 100-kN load frame with hydraulic grips for all our experiments, it is likely that such movement was minimal and not even as large as the Poisson contraction. Thus, it seems reasonable to assume that the overall strain error was no larger than a few thousand microstrains. Although this may be a very large error for infinitesimal deformation measurements, it is worth noting that in our work, we are interested exclusively in failure strains, which range from 40–110 % in our experiments. Therefore, we conclude that the strain errors that occur because of out-of-plane motion of the specimen surface do not affect our results or conclusions significantly.

COMPUTATION OF STRESS

The stress experienced by the specimen was computed from the load data obtained from the tensile testing machine. Approximately 100 load values were recorded per second while only one image was captured per second. Hence, every image was correlated to the mean value of the load data recorded in one second. In this study, two different values of stresses were computed: (a) engineering stress, σ_{engg}, computed using the residual cross-sectional area at the FL measured at the beginning of the test, and (b) true stress, σ_{true}, computed using the actual cross-sectional area at the FL at that particular instant of time (taking into account the instantaneous reduction in the cross-sectional area as the specimen deforms under stress).

The residual cross-sectional area at the FL at the beginning of the test was obtained using the 3D laser scanning technique. However, it is a challenging task to measure the instantaneous reduction in the cross-sectional area as the specimen deforms. Roesler, Harders, and Baeker [26] have provided a method to compute the instantaneous reduction in the cross-sectional area.

In materials with plastic deformation much higher than elastic deformation, if the strain can be measured very close to the FL, the instantaneous reduction in the cross-sectional area at the FL can be computed assuming conservation of the volume of the deforming specimen. Roesler, Harders, and Baeker [26] have stated that this assumption is acceptable in the case of metals. In this study, the true stress at the FL was computed using this assumption, with the understanding that this assumption is not a good one till the yield point but is justified for the larger strains at failure. Up to the proof stress, the true stress in the specimen was computed using a Poisson's ratio of 0.287, which corresponds to that of cold-rolled steel. As per assumption of volume conservation, Eq 4 can be formulated as follows:

$$A_0 \times h_0 = A_n \times h_n \tag{4}$$

where:

A_0 = the initial cross-sectional area at the beginning of the test (measured from the 3D model of the specimen),

h_0 = a length of a segment including the FL, which was taken as 1 mm in this study,

A_n = the actual cross-sectional area at any instant of time n, and

h_n = the deformed length of the segment h_0 at n. The deformed length of the segment, h_n, was computed using Eq 5,

$$h_n = h_0(1+\varepsilon_{FL}) \tag{5}$$

where:

ε_{FL} is the strain at FL at n. A_n can be computed using the above Eq 4 as the other three variables are known. True stress at every instant of time, n, is calculated as given in Eq 6:

$$\sigma_{true,n} = \frac{P_n}{A_n} \tag{6}$$

Thus, using the computed values of stress and strain values, two different stress-strain curves are plotted for the test specimens: (a) the engineering stress-strain curve, denoted as $\sigma_{engg} - \varepsilon_{FL}$, and (b) the true stress-strain curve, denoted as $\sigma_{true} - \varepsilon_{FL}$. It should be noted that all the plotted stress-strain curves and the evaluated mechanical properties in this study correspond to the FL of the specimen, unless specified otherwise. **Fig. 9** shows a flowchart briefly describing the processes explained in the sections "Preparation of Test Specimens" through "Computation of Stress."

FIG. 9 Steps involved in the proposed test and evaluation method.

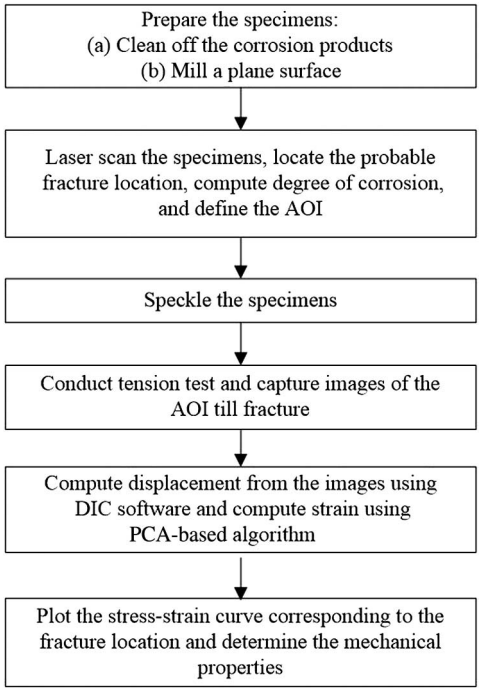

STUDY OF STRESS-STRAIN BEHAVIOR AND STRAIN DISTRIBUTION

The feasibility of the proposed method is determined using the four specimens, as detailed in "Phase I: Development of Test and Evaluation Method." Using the proposed technique, the stress-strain behavior and the strain distribution along the length of the specimen were assessed. **Fig. 10** presents the engineering and true stress-strain curves plotted for the control PM steel rebar (S0) and CTD rebar specimen with 3 % degree of corrosion (S1) at the FL. Using the proposed method, the strain distribution at different points along the length of the specimen was assessed.

Fig. 11 shows the stress-strain curve at different points along the length of the specimen, 5 mm apart, including the FL. The longest stress-strain curve corresponds to the FL and the curves to the left corresponding to the locations 5, 10, 15, 20, 25, and 30 mm away from FL, marked as A to F on the specimen.

Fig. 11a exhibits the stress-strain curves plotted for points along the PM steel rebar specimen with negligible corrosion. The strain at the FL reaches 0.8, the strain at a point A (5 mm away from the FL) reaches 0.6, while the stresses at all the regions further away drops at a strain of approximately 0.2. A comparison of **Fig. 11b–d**, corresponding to the three corroded CTD rebars, shows that ultimate strain at the FL varies for these specimens, and the relative position of stress-strain curves for points A, B, C, D, E, and F with respect to that corresponding to FL is different for each of these specimens. For instance, the FL as well as points A and B show considerable strains with respect to

FIG. 10 Engineering and true stress-strain curves obtained using the proposed method.

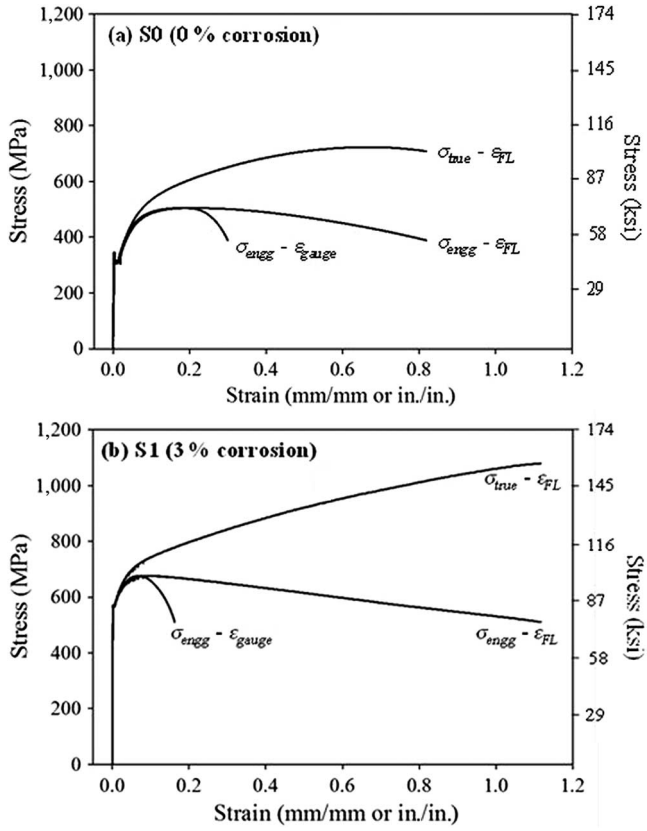

the locations further away in the CTD steel rebar specimen with 18 % corrosion. On the other hand, the strain at the FL in the specimen with 33 % corrosion is similar to that in the specimen with 3 % corrosion. However, the regions away from the FL in the specimen with 33 % corrosion show lower strain than the corresponding points in the specimen with 3 % corrosion. This indicates that there is considerable strain heterogeneity along the length of the rebar specimens. The strain heterogeneity varies from specimen to specimen and depends more on the cross-sectional area than on the degree of corrosion. This reiterates the need for a full-field deformation technique to understand the deformation in corroded rebars.

Phase II: Evaluation of Stress-Strain Behavior of Corroded Rebars Using the Developed Method

This section presents the results obtained after evaluation of mechanical properties of corroded rebars using the developed method. The data points in the graphs provided in this section have been replaced by the specimen IDs for more clarity.

FIG. 11 Stress-strain curves at different locations along the length of the rebar specimens indicating the influence of variability in cross-sectional area in the strain distribution: (a) S0 (0 % corrosion), (b) S1 (3 % corrosion), (c) S4 (18 % corrosion) and (d) S12 (33 % corrosion).

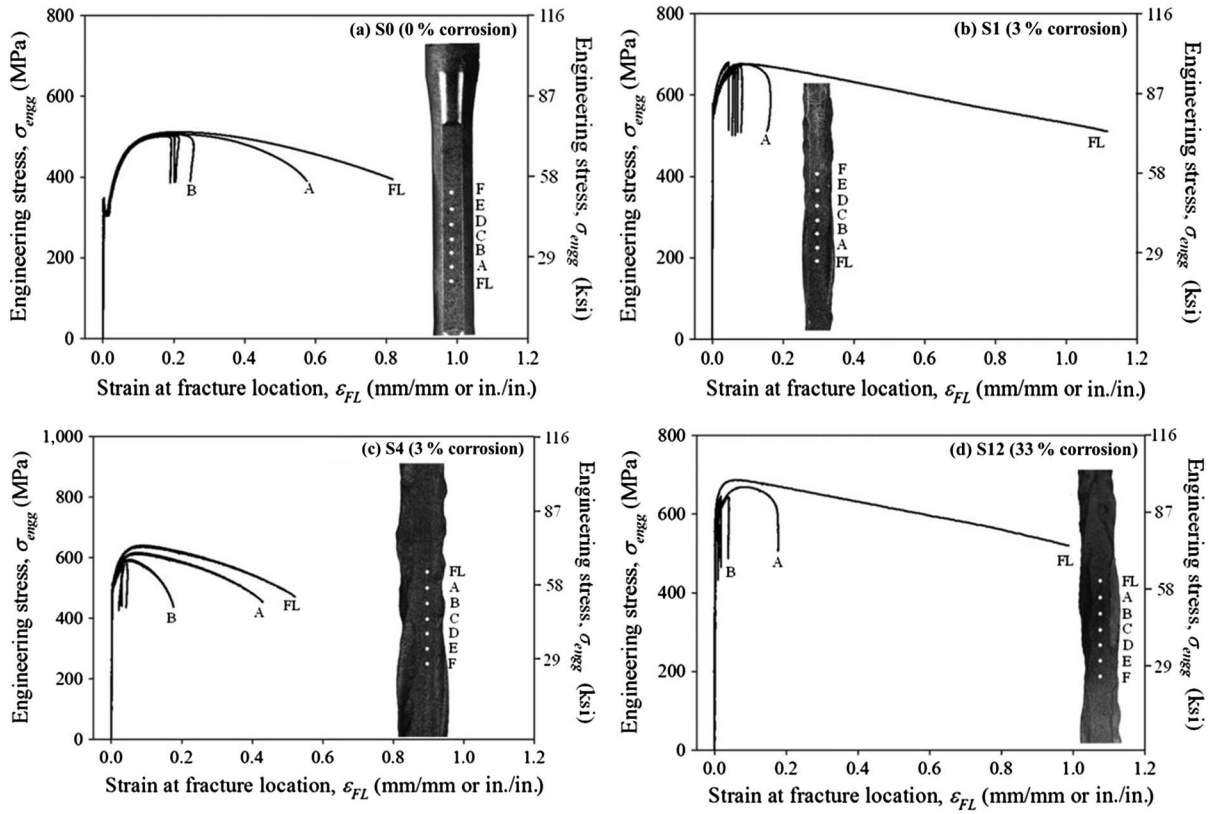

Fig. 12a and **12b** shows the engineering and true stress-strain graphs of all 13 CTD rebar specimens. For clarity, the stress-strain curves of the 13 specimens are provided in two separate plots, S1–S7 (3–24 % corrosion) and S8–S13 (25–40 % corrosion). The sudden drop close to fracture observed in the stress-strain curves of Specimens S5, S8, and S10 could be due to the initiation of fracture at the rear side of the specimen (which is not captured by the camera placed on the other side).

Table 7 presents the computed proof stress, ultimate strength, and ultimate strain (over 60 mm or 2.362 in.) gauge length and at the FL of all the 13 CTD rebar specimens. It should be noted that the data points might appear as two clusters in the plots, as there are no specimens with degree of corrosion in between 3–18 %.

EFFECT OF CORROSION ON PROOF STRESS

In this study, the yield strength of the CTD rebar specimens is defined as the offset yield point (proof stress) corresponding to 0.2 % plastic strain because, unlike PM steel, CTD steel does not exhibit a definite yield point in the stress-strain curve. In this article, the proof stress of the CTD rebar specimens is denoted as σ_p. **Fig. 13a** shows the variation in σ_p with increasing degree of corrosion. The values of σ_p of the 13 specimens range from approximately 540–680 MPa (78.320–98.625 ksi) (refer to **Table 7** for more details). The plot shows no visible trend of variation in proof stress with increasing degree of corrosion.

A statistical analysis was carried out on the proof stress data using Student's *t*-test (assuming the data to be normally distributed) to determine whether the data was statistically similar to conclude that corrosion has no significant effect on the proof stress of the rebars. The null hypothesis is that corrosion has no effect on the σ_p of CTD rebar specimens. The specimens were divided into two groups based on degree of corrosion, one with very low level of corrosion (<5 % corrosion) and another with significant level of corrosion (5–40 % corrosion). A one-tailed *t*-test for two sets of data with unequal sample size and unequal variance for $\alpha = 0.1$ gave a *p*-value of 0.154 (>0.05), which indicates that the null hypothesis, corrosion has no significant effect on the σ_p of rebars, can be accepted. Also, the coefficient of variation of the data is 0.076, which is acceptable. It should be acknowledged that the *t*-test may give conservative results for a low sample size of 3 and 10 specimens.

EFFECT OF CORROSION ON ULTIMATE STRENGTH

The ultimate strength is computed as the stress experienced by the specimen at the peak load and is denoted as σ_u. **Fig. 13b** shows

FIG. 12 Engineering and true stress-strain curves of corroded CTD specimens: (a) S1–S7 (3–23 % corrosion) and (b) S8–S13 (25–40 % corrosion).

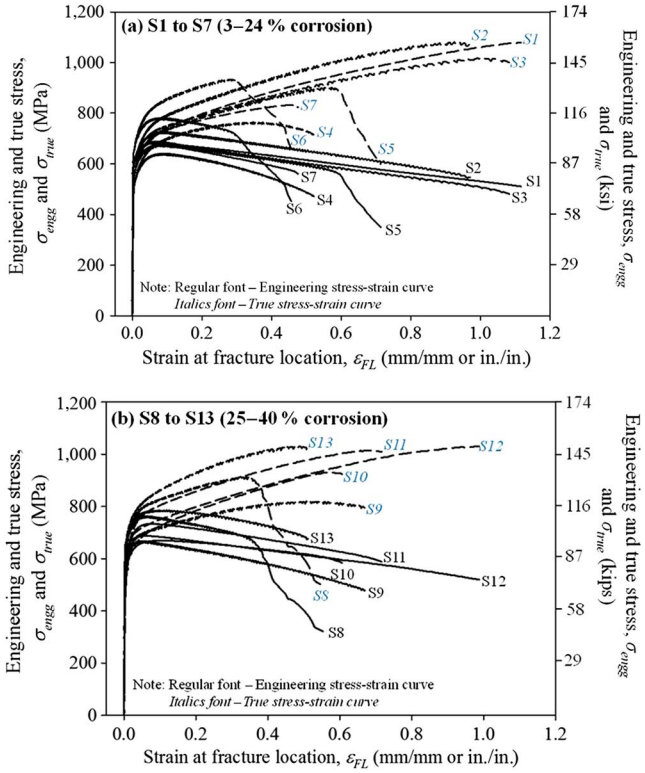

TABLE 7 Mechanical properties of corroded test specimens estimated using the developed method.

Specimen ID	Degree of Corrosion (%)	Proof Stress, σ_p (MPa)	Ultimate Strength, σ_u (MPa)	Ultimate Strain at Fracture Location, $\varepsilon_{FL,ult}$ (%)
1	3	569	676	112
2	4	602	725	97
3	4	592	688	109
4	18	538	640	52
5	18	577	674	71
6	23	665	780	46
7	24	587	680	48
8	28	658	762	55
9	30	542	667	67
10	31	588	669	72
11	32	600	733	99
12	33	642	687	51
13	40	682	784	61

the variation of σ_u of the rebars computed using A_{FL} with increasing degree of corrosion. The plot does not exhibit any visible trend in the variation of σ_u with increasing degree of corrosion.

FIG. 13 Effect of corrosion on strength properties of unstressed CTD steel rebars: (a) proof stress (σ_p) and (b) ultimate strength (σ_U).

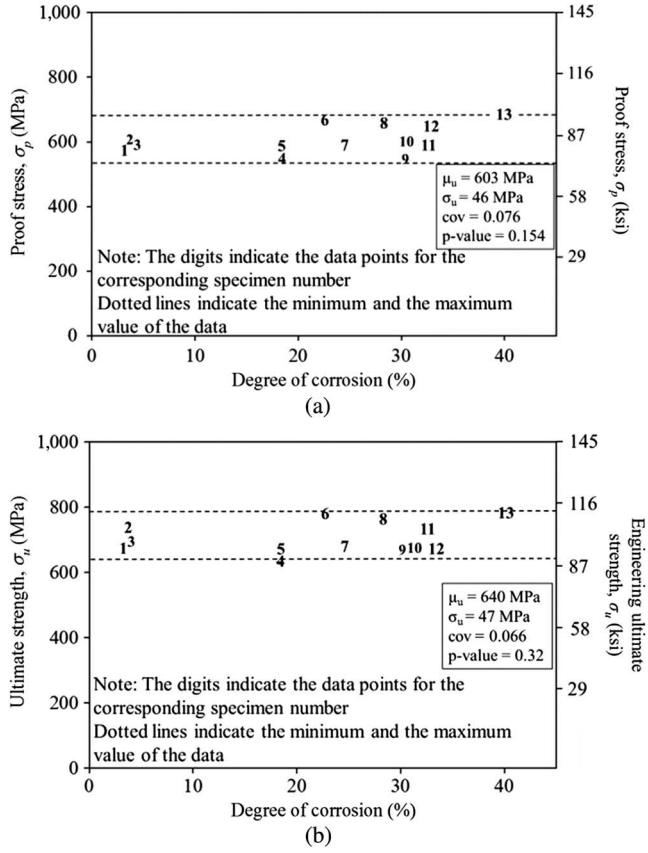

The σ_u values of the 13 CTD rebar specimens ranges from approximately 640 to 780 MPa (92 to 113 ksi) (see **Table 7**).

A Student's *t*-test was conducted on this data as well, grouped into two categories, < 5 % and 5–40 % degree of corrosion, to determine the statistical significance of the observed effect of corrosion on σ_u. A one-tailed *t*-test for two sets of data with unequal sample size and unequal variance gave a *p*-value of 0.32, which is greater than $\alpha = 0.1$. This suggests that the null hypothesis that corrosion does not have a significant effect on σ_u is acceptable. Also, the coefficient of variation in the data is 0.066, which is acceptable. It should be noted that the load capacity of rebars (in kN) might decrease because of reduction in the cross-sectional area. However, this study shows that the strength properties of the residual intact steel are not significantly affected for unstressed CTD rebar specimens.

EFFECT OF CORROSION ON ULTIMATE STRAIN

Conventionally, the ductility of corroded rebars is expressed in terms of the effective strain (measured over the gauge length) exhibited by the specimens at fracture. In this study, ultimate strain or strain at fracture is measured over the gauge length as well as at

FIG. 14 Effect of corrosion on the ultimate strain (ductility) of unstressed corroded CTD rebars: (a) variation in $\varepsilon_{gauge,ult}$ with increasing degree of corrosion and (b) variation in $\varepsilon_{FL,ult}$ with increasing degree of corrosion.

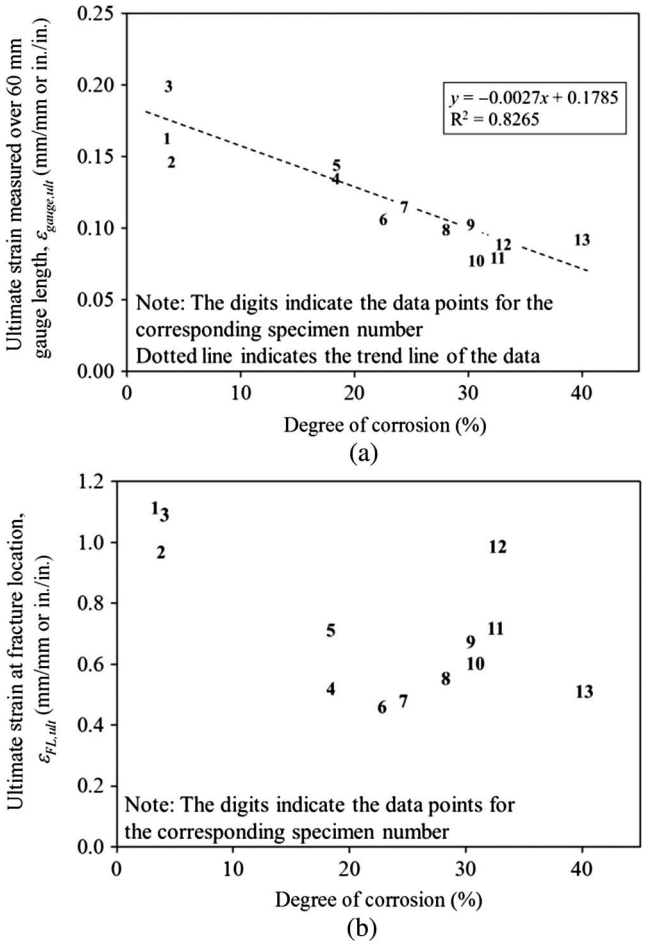

the FL (over 15 pixels length, which is approximately 0.8–1 mm for different specimens), and these are denoted as $\varepsilon_{gauge,ult}$ and $\varepsilon_{FL,ult}$, respectively. **Fig. 14a** shows the variation in $\varepsilon_{gauge,ult}$ of 13 CTD rebar specimens with increasing degree of corrosion. $\varepsilon_{gauge,ult}$ shows a decreasing trend with increasing degree of corrosion. This observed reduction is due to the uneven surface topology of corroded rebars causing stress-concentration at the location with the least cross-sectional area (i.e., the FL), which leads to localization of the strain. Consequently, the strain computed using an extensometer has a lower average value, which explains the observed reduction in ductility because of corrosion. **Fig. 14b** shows the variation in the ultimate strain measured at the FL, $\varepsilon_{FL,ult}$, with increasing degree of corrosion. For Specimens 1–7, the ultimate strain measured at FL is qualitatively similar to that seen in the ultimate strain plots using 60-mm gauge length. However, for Specimens 8–13, there is much more scatter in the ultimate strain measured at the FL compared to those from the 60-mm gauge length calculation. It is worth noting that the local strain values are based on 2D-DIC, and the actual 3D shape of the specimen in the thickness direction and its influence on the resulting deformation are unknown. Thus, it is not possible to draw any firm conclusions from the ultimate strain computations. In order to understand these differences more clearly and link them to the observed deformations, one would need to use the more accurate 3D-DIC analysis.

Conclusions

This article proposes a refined method for assessing the stress-strain behavior of corroded rebars with uneven cross-sectional area using DIC technique. The study is conducted in two phases: (a) development of the testing and evaluation method and (b) evaluation of the effect of corrosion on mechanical properties of corroded CTD rebars using the develop method. A feasibility study using a control PM steel rebar of uniform cross-sectional area and corroded CTD rebars with uneven cross-sectional area. The feasibility study showed that the proposed method can assess the local mechanical properties at FL and the strain distribution along the AOI, which gives a better estimate and understanding of the effect of corrosion on the stress-strain behavior.

The stress-strain behavior of a set of unstressed CTD steel rebars having degree of corrosion ranging from 3–40 % was evaluated using the proposed method. This part of the study showed that the proof stress and the ultimate strength of the residual intact steel are not affected by corrosion. The ductility of the rebars was evaluated in terms of ultimate strain measured over 60-mm gauge length using the conventional method as well as at the FL using DIC; the magnitude of strain measured with the latter was significantly different from that measured with the former. This difference in estimated strain magnitudes can be directly traced to the heterogeneity in the underlying deformation that is caused by the non-uniform geometry of the rebar. This observation emphasizes the need for more accurate measurement and prediction of FL and computation of strain at the FL for an accurate assessment of stress-strain behavior of corroded rebars. This initial study shows that DIC is a promising technique that can be used to obtain true local deformation and hence the true stress-strain behavior of corroded rebars, without the ambiguity associated with the gauge length.

APPLICATIONS

This method for corroded rebars can create a good backup of the test data, especially a 3D virtual model of the test specimen and all the deformation data stored as images. These data can be used for further analysis of the test data even though the specimen is broken. This method can be applied for forensic investigation of structures.

LIMITATIONS AND RECOMMENDATIONS FOR FUTURE WORK

The developed test method for assessing the stress-strain behavior of corroded rebars has the following limitations:

- The measurement of the displacements in the specimens over a plane surface using 2D-DIC may lead to less accurate results after the commencement of the test because of rotations and out-of-plane deformations, especially after necking.
- Milling of the specimen to obtain a plane surface may induce geometrical variations in the specimen by removing a part of the corroded surface.

The limitations of these methods can be overcome with 3D-DIC, which uses two cameras in a stereo rig to reconstruct the 3D surface accurately and correlate such surfaces at different time instances to estimate surface deformations. The use of 3D-DIC may demand more expertise in the technique; however, higher accuracy can be achieved, and complicated specimen preparation procedure can be avoided.

The scope of the future work is as follows:

- Understanding the stress-strain behavior of stressed rebars using the developed method.
- Assessment of the stress-strain behavior of corroded rebars using 3D-DIC to obtain more accurate and reliable estimation of the strain.

ACKNOWLEDGMENTS

The authors are thankful for the technical support for this study from the Department of Civil Engineering, the Department of Engineering Design, and the Department of Metallurgical and Materials Engineering, all at the Indian Institute of Technology (IIT) Madras, Chennai, India. The financial support from the FIST scheme (Grant No. ETII/054/2012) of Department of Science and Technology (DST) and the Ministry of Human Resources Development (MHRD), Government of India through IIT Madras is greatly appreciated. The authors are also thankful to Prof. Ravindra Gettu for the technical guidance offered.

References

[1] Du, Y. G., Clark, L. A., and Chan, A. H. C., "Residual Capacity of Corroded Reinforcing Bars," *Mag. Concr. Res.*, Vol. 57, No. 3, 2005, pp. 135–147, https://doi.org/10.1680/macr.2005.57.3.135

[2] Taha, N. A. and Morsy, M., "Study of the Behavior of Corroded Steel Bar and Convenient Method of Repairing," *HBRC J.*, Vol. 12, No. 2, 2016, pp. 107–113, https://doi.org/10.1016/j.hbrcj.2014.11.004

[3] Almusallam, A. A., "Effect of Degree of Corrosion on the Properties of Reinforcing Steel Bars," *Constr. Build. Mater.*, Vol. 15, No. 8, 2001, pp. 361–368, https://doi.org/10.1016/S0950-0618(01)00009-5

[4] Apostolopoulos, C. A. and Papadakis, V. G., "Consequences of Steel Corrosion on the Ductility Properties of Reinforcement Bar," *Constr. Build. Mater.*, Vol. 22, No. 12, 2008, pp. 2316–2324, https://doi.org/10.1016/j.conbuildmat.2007.10.006

[5] François, R., Khan, I., and Dang, V. H., "Impact of Corrosion on Mechanical Properties of Steel Embedded in 27-Year-Old Corroded Reinforced Concrete Beams," *Mater. Struct.*, Vol. 46, No. 6, 2013, pp. 899–910, https://doi.org/10.1617/s11527-012-9941-z

[6] Cairns, J., Plizzari, G. A., Yinyang, D., Law, D. W., and Franzoni, C., "Mechanical Properties of Corrosion-Damaged Reinforcement," *ACI Mater. J.*, Vol. 102, No. 4, 2005, pp. 256–264.

[7] Palsson, R. and Mirza, S. M., "Mechanical Response of Corroded Steel Reinforcement of Abandoned Concrete Bridge," *Struct. J.*, Vol. 99, No. 2, 2002, pp. 157–162.

[8] Du, Y. G., Clark, L. A., and Chan, A. H. C., "Effect of Corrosion on Ductility of Reinforcing Bars," *Mag. Concr. Res.*, Vol. 57, No. 7, 2005, pp. 407–419, https://doi.org/10.1680/macr.2005.57.7.407

[9] Lee, H.-S. and Cho, Y.-S., "Evaluation of the Mechanical Properties of Steel Reinforcement Embedded in Concrete Specimen as a Function of the Degree of Reinforcement Corrosion," *Int. J. Fract.*, Vol. 157, Nos. 1–2, 2009, pp. 81–88, https://doi.org/10.1007/s10704-009-9334-7

[10] Zhu, W. and François, R., "Effect of Corrosion Pattern on the Ductility of Tensile Reinforcement Extracted from a 26-Year-Old Corroded Beam," *Adv. Concr. Constr.*, Vol. 1, No. 2, 2013, pp. 121–136, https://doi.org/10.12989/acc2013.01.2.121

[11] ASTM E8/E8M, *Standard Test Methods for Tension Testing of Metallic Materials* (Superseded), ASTM International, West Conshohocken, PA, 2013, www.astm.org

[12] Kashani, M. M., Crewe, A. J., and Alexander, N. A., "Use of a 3D Optical Measurement Technique for Stochastic Corrosion Pattern Analysis of Reinforcing Bars Subjected to Accelerated Corrosion," *Corros. Sci.*, Vol. 73, 2013, pp. 208–221, https://doi.org/10.1016/j.corsci.2013.03.037

[13] Apostolopoulos, C. A., Demis, S., and Papadakis, V. G., "Chloride-Induced Corrosion of Steel Reinforcement – Mechanical Performance and Pit Depth Analysis," *Constr. Build. Mater.*, Vol. 38, 2013, pp. 139–146, https://doi.org/10.1016/j.conbuildmat.2012.07.087

[14] Sutton, M. A., Orteu, J. J., and Schreier, H., *Image Correlation for Shape, Motion and Deformation Measurements: Basic Concepts, Theory and Applications*, Springer US, New York, NY, 2009, pp. 127–137.

[15] Malesa, M., Szczepanek, D., Kujawińska, M., Świercz, A., and Kołakowski, P., "Monitoring of Civil Engineering Structures Using Digital Image Correlation Technique," presented at the *14th International Conference on Experimental Mechanics*, Poitiers, France, July 4–9, 2010, European Society for Experimental Mechanics, France, https://doi.org/10.1051/epjconf/20100631014

[16] Gencturk, B., Hossain, K., Kapadia, A., Labib, E., and Mo, Y. L., "Use of Digital Image Correlation Technique in Full-Scale Testing of Prestressed Concrete Structures," *Measurement*, Vol. 47, 2014, pp. 505–515, https://doi.org/10.1016/j.measurement.2013.09.018

[17] Li, X. Y. and Zhang, Z. G., "The Impact of Corrosion on the Mechanical Properties of Smooth Steel Rebar HPB235," *Adv. Mater. Res.*, Vols. 179–180, 2011, pp. 28–31, https://doi.org/10.4028/www.scientific.net/AMR.179-180.28

[18] McCormick, N. and Lord, J., "Digital Image Correlation," *Mater. Today*, Vol. 13, No. 12, 2010, pp. 52–54, https://doi.org/10.1016/S1369-7021(10)70235-2

[19] Pan, B., Qian, K., Xie, H., and Asundi, A., "Two-Dimensional Digital Image Correlation for In-Plane Displacement and Strain Measurement: A Review," *Meas. Sci. Technol.*, Vol. 20, No. 6, 2009, 062001, https://doi.org/10.1088/0957-0233/20/6/062001

[20] Bornert, M., Brémand, F., Doumalin, P., Dupré, J. C., Fazzini, M., Grédiac, M., Hild, F., Mistou, S., Molimard, J., Orteu, J. J., Robert, L., Surrel, Y., Vacher, P., and Wattrisse, B., "Assessment of Digital Image Correlation Measurement Errors: Methodology and Results," *Exp. Mech.*, Vol. 49, No. 3, 2009, pp. 353–370, https://doi.org/10.1007/s11340-008-9204-7

[21] David, M. R., "A Simple Autocorrelation Algorithm for Determining Grain Size from Digital Images of Sediment," *J. Sediment. Res.*, Vol. 74, No. 1, 2004, pp. 160–165, https://doi.org/10.1306/052203740160

[22] Grama, S. N. and Subramanian, S. J., "Computation of Full-field Strains Using Principal Component Analysis," *Exp. Mech.*, Vol. 54, No. 6, 2014, pp. 913–933, https://doi.org/10.1007/s11340-013-9800-z

[23] Reu, P., "Virtual Strain Gage Size Study," *Exp. Tech.*, Vol. 39, No. 5, 2015, pp. 1–3, https://doi.org/10.1111/ext.12172

[24] Sharma, S., Vinuchakravarthy, S., and Subramanian, S. J., "Estimation of Surface Curvature from Full-Field Shape Data Using Principal Component Analysis," *Meas. Sci. Technol.*, Vol. 28, No. 1, 2017, 015003, https://doi.org/10.1088/0957-0233/28/1/015003

[25] Sutton, M. A., Yan, J. H., Tiwari, V., Schreier, H. W., and Orteu, J. J., "The Effect of Out-of-Plane Motion on 2D and 3D Digital Image Correlation Measurements," *Opt. Lasers Eng.*, Vol. 46, No. 10, 2008, pp. 746–757, https://doi.org/10.1016/j.optlaseng.2008.05.005

[26] Roesler, J., Harders, H., and Baeker, M., *Mechanical Behaviour of Engineering Materials: Metals, Ceramics, Polymers, and Composites*, Springer, Berlin, Germany, 2007, pp. 73–81.